APPLIED PHYSICS LETTERS

Polar-surface dominated ZnO nanobelts and the electrostatic energy induced nanohelixes, nanosprings, and nanospirals

Xiang Yang Kong[a)] and Zhong Lin Wang[b)]
School of Materials Science and Engineering, Georgia Institute of Technology, Atlanta, Georgia 30332-0245

We report the controlled synthesis of free-standing ZnO nanobelts whose surfaces are dominated by the large polar surfaces. The nanobelts grow along the *a* axis, their large top/bottom surfaces are the $\pm(0001)$ polar planes, and the side surfaces are $(01\bar{1}0)$. Owing to the positive and negative ionic charges on the zinc- and oxygen-terminated $\pm(0001)$ surfaces, respectively, the nanobelts form multiloops of nanohelixes/nanosprings/nanospirals for the sake of reducing electrostatic energy introduced by the polar surfaces as well as balancing the difference in surface tension. The polar surface dominated ZnO nanobelts are likely to be an ideal system for understanding piezoelectricity and polarization induced phenomena at nanoscale. © *2004 American Institute of Physics.* [DOI: 10.1063/1.1646453]

Considerable research effort was focused recently on quasi-one-dimensional (1-D) nanomaterials,[1] due to their potential applications as building blocks for nanocircuits,[2] nano-optoelectronics,[3] and nanosensors.[4,5] In literature, the 1-D nanomaterials are termed diversely as nanowires, nanorods, nanoribbons, nanobelts, etc. Among these terminologies, the remarkable characteristics of the nanobelts are the well-defined facets, unique growth direction, and a typical rectangular cross section.[6] Simply, nanobelt is a structurally controlled nanowire structure. It is possible that facet control on nanowire may have equivalent importance as the control over the helical angle of a single-walled carbon nanotube, which determines its semiconductor or metallic characteristic.

Zinc oxide (ZnO) is a versatile smart material that has key applications in catalysts, sensors, piezoelectric transducers,[7] transparent conductor and surface acoustic wave devices.[8] ZnO has wurtzite structure which is described schematically as a number of alternating planes composed of fourfold coordinated O^{2-} and Zn^{2+} ions, stacked alternatively along the *c* axis. ZnO has partial ionic characteristics, thus there is a net dipole moment along the *c* axis. For the basal planes, the (0001) plane is terminated by Zn and $(000\bar{1})$ plane terminated by O, resulting in the divergence of surface energy for large polar surfaces. The other commonly observed planes of $\{01\bar{1}0\}$ and $\{2\bar{1}\bar{1}0\}$ are nonpolar planes, which have lower surface energy compared to the polar basal plane. The crystallographic anisotropy of ZnO results in anisotropic growth. Under thermodynamic equilibrium condition, the facet with higher surface energy is usually small in area, while the lower energy facets are larger. Specifically in the ZnO growth, the highest growth rate is along the *c* axis and the large facets are usually $\{01\bar{1}0\}$ and $\{2\bar{1}\bar{1}0\}$.[6,9,10] In this article, we show that, by controlling growth kinetics, it is possible to change the growth behavior of ZnO nanobelts.

We report free-standing ZnO nanobelts whose large top/bottom flat surfaces are the $\pm(0001)$ polar surfaces. As a result of surface polarization, nanohelixes are formed to reduce the electrostatic energy. This type of polar surface dominated 1-D nanostructure could have potential applications as nanosensors and nanotransducers.

The facet controlled ZnO nanobelts with polar surface were synthesized by a solid–vapor process.[6] Zinc oxide powders with 1% Li_2O were placed at the highest temperature zone of a tube furnace. Before heating to the desired temperature of 1350 °C, the tube furnace was evacuated to $\sim10^{-3}$ Torr to remove the residual oxygen. Then the source materials were heated to 1350 °C at a heating rate of 20 °C/min. ZnO decomposes into Zn^{2+} and O^{2-} at high temperature (1350 °C) and low pressure ($\sim10^{-3}$ Torr), and this decomposition process is the kinetic control step for producing the *c*-plane nanobelts, which is different from the growth process used for synthesizing the nanobelts.[6] The growth condition is in nonequilibrium state, the anisotropic growth rate is different in thermodynamic equilibrium state. After a few minutes of evaporation and decomposition, the Ar carrier gas was introduced at a flux of 25 sccm. The growth was conducted at 1350 °C for 30 min. The nanobelts were grown on the alumina substrate placed in a temperature zone of 400–500 °C under Ar pressure of 250 Torr. Structures of the ZnO nanobelts were analyzed by scanning electron microscopy (SEM, LEO 1530 FEG at 5 kV), high-resolution transmission electron microscopy (HRTEM, Hitachi HF-2000 FEG at 200 kV and JEOL 4000EX at 400 kV).

SEM images show that the as-received product has a belt-shape with widths of 10–60 nm, thickness of 5–20 nm, and lengths up to several hundreds of micrometers, much smaller than the widths and thickness of the *c*-axis nanobelts reported previously.[6] The dominant component of the as-synthesized sample is nanobelts with a uniform size distribution between 20 and 30 nm. [Fig. 1(a)]. The most striking character of the sample is the formation of helical nanosprings/nanohelixes by rolling up a single-crystalline nanobelt [Fig. 1(b)]. The nanospring has a uniform structure
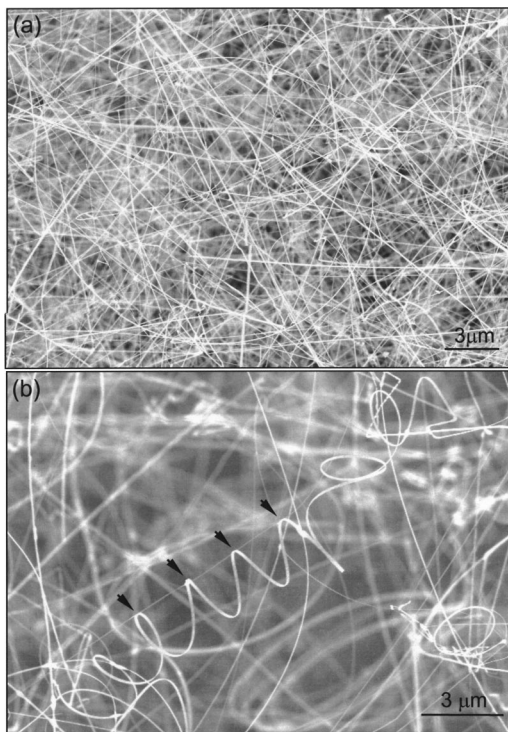

FIG. 1. (a) SEM images of the as-synthesized ZnO nanobelts with high uniformity and purity. (b) A SEM image displaying the helical nanosprings found in the sample. The width of the nanobelt is ~20–30 nm.
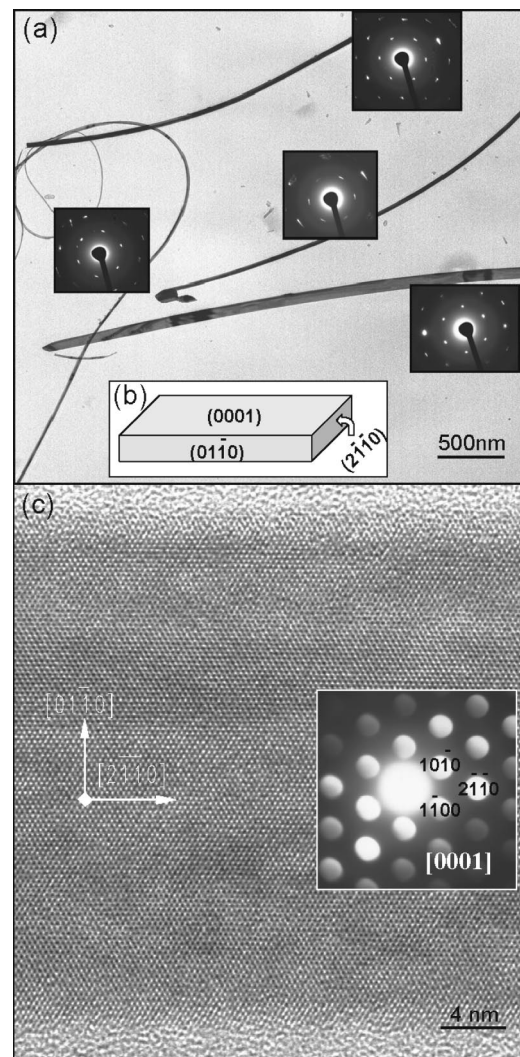

FIG. 2. A typical, unselected low magnification TEM image, showing four ZnO nanobelts laid down onto a carbon substrate and the corresponding electron diffraction patterns recorded from them. All of the nanobelts shown here have a large (0001) surface that is closely parallel to the direction of the incident electron beam. (b) Structure model of the ZnO nanobelt. (c) High-resolution TEM image and the corresponding electron diffraction pattern recorded from a ZnO nanobelt, showing single-crystal, dislocation-free volume.

with radii of ~500–800 nm and evenly distributed pitches.

The ZnO nanobelt has a controlled structure. By examining over hundreds of nanobelts laid down naturally onto a carbon film by electron diffraction without tilting the specimen, almost all of them show the same orientation of [0001] with respect to the incident electron beam. Figure 2(a) shows a few local diffraction patterns recorded from a few nanobelts deposited onto a carbon film. All four of the nanobelts are oriented with c plane upward, indicating that the top flat surface of the nanobelts is (0001) plane and the polar surface controlled synthesis has been achieved. The ZnO nanobelt has a hexagonal wurtzite structure. Electron diffraction proves that the nanobelt grows along $[2\bar{1}\bar{1}0]$ (the a axis), with its top/bottom surface $\pm(0001)$ and the side surfaces $\pm(01\bar{1}0)$ [Fig. 2(b)]. HRTEM shows that the nanobelt is single crystalline without the presence of dislocations [Fig. 2(c)], and its geometrical shape is uniform. The surfaces of the nanobelt are clean and atomically sharp and flat.

Since the ZnO $(2\bar{1}\bar{1}0)$ has a lower surface energy than that of (0001), a fast growth along $[2\bar{1}\bar{1}0]$ (a axis) to form the c-plane dominated nanobelt may be unfavorable from the energy point of view. But the success of controlled growth along the a axis with >90% yield demonstrated here shows that controlling growth kinetics and experimental conditions can overcome the barrier placed by surface energy in nanostructure growth, thus, opening a new channel for growth of structurally controlled nanobelts of technological importance.

The polar surface dominated nanobelt exhibits a unique structure feature: the formation of helical nanosprings [Figs. 3(a) and 3(b)]. Helical structures have been found using SEM [Fig. 3(c)] and TEM [Fig. 3(d)]. This structure is a result of growth rather than specimen handling or twisting

postgrowth. To understand this phenomenon, we need to examine the characteristic of the polar surfaces. Our analysis shows that the ZnO nanobelt is faceted with polar planes $\pm(0001)$ (the top and bottom surfaces) and nonpolar $\pm(2\bar{1}\bar{1}0)$ (front and end surfaces) and the $\pm(01\bar{1}0)$ (side surfaces) planes. The three types of planes are the most stable facets for wurtzite structured ZnO and exhibit no surface reconstruction. The (0001) plane can be terminated with Zn [(0001)-Zn] or oxygen [(000$\bar{1}$)-O], resulting in positively and negatively charged top and bottom surfaces [Fig. 4(a)], respectively. If the surface charges are uncompensated, the net dipole moment tends to diverge and the electrostatic potential increases. For a thin nanobelt laying on a substrate, the spontaneous polarization induces electrostatic energy due to the dipole moment, but a rolling up to form a circular ring would minimize or neutralize the overall dipole moment [Fig. 4(b)], reducing the electrostatic energy. This is supported by the multiloops of nanorings observed in Figs. 2(a) and 2(b). On the other hand, bending of a single crystalline
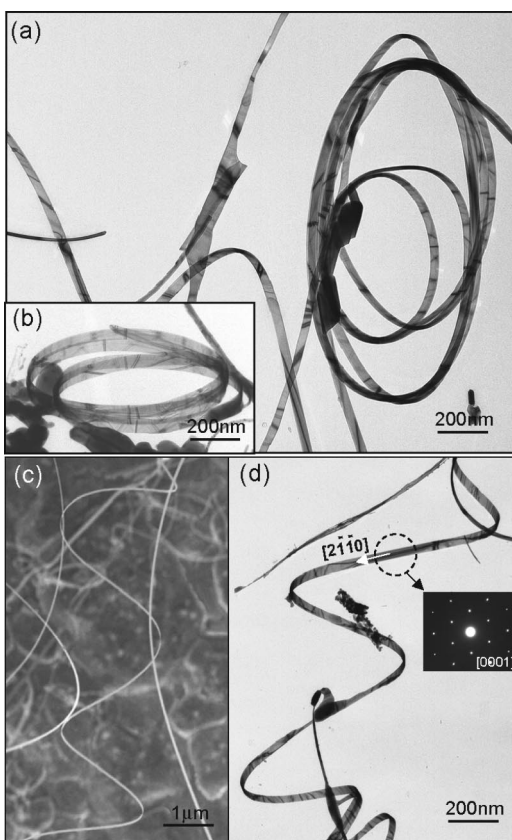
FIG. 3. (a), (b) Multiloop helical structures of the ZnO nanobelt. The nanobelt is rolled with its *c* axis pointing toward the center of the helix. (c) SEM image of a helical twisting structure, and (d) a TEM image of the structure, which is made of a single-crystal ZnO nanobelt.

nanobelt produces elastic energy. The stable shape of the nanobelt is determined by the minimization of the total energy contributed by spontaneous polarization and elasticity. Due to the small thickness of 5–20 nm and large aspect ration of ~1:4, the flexibility and toughness of the nanobelts are extremely high so that it can be bent or twisted without fracture or creating dislocations. If the nanobelt is so thin
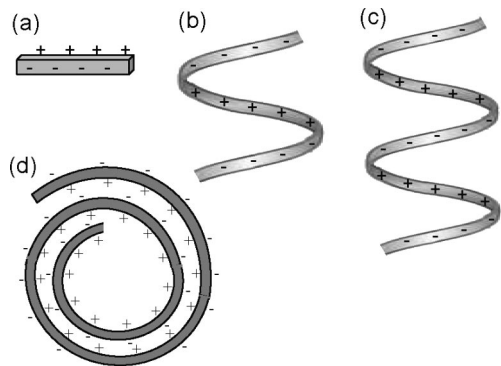

FIG. 4. Formation process of a nanobelix. (a) Nanobelt with positively and negatively charged top and bottom surfaces, respectively. There is a dipole moment across the thickness of the nanobelt. (b) The nanobelt is rolled up to form a ''ring'' structure to eliminate the dipole moment. (c) A continuous growth of the nanobelt leads to the formation of nanohelix/nanospring. The model shown here assumes that the positive charges are on the inner surface and the negative charges are on the exterior surface.

that a decrease in electrostatic energy after rolling up a straight nanobelt into a helical spring or ring is larger than the elastic energy induced by the bending, a stable helical spring or ring would be formed; otherwise, the nanobelt remains as a straight entity. Naturally, multiple loops of nanorings are formed, as shown in Fig. 2(a). On the other hand, the bending of the nanobelt proceeds during the growth along the axial direction of the nanobelt, naturally forms the helical structure [Fig. 4(c)]. This is evidenced by the SEM image shown in Fig. 1(b), where the enclosing and wiring of the helical nanobelt around a straight nanobelt is presented, as indicated by arrowheads. Another factor that may contribute to the helical formation is the difference in surface tensions on the Zn- and O-terminated surfaces.[11] *In situ* TEM observation found that the helical structure is stable even after heating to 800 °C in vacuum. A calculation based on the first principle is required to evaluate the contributions made by different processes. It must be pointed out that *the nanosprings made of a single crystal have only been observed for the polar surface dominated ZnO*. The nanosprings formed for amorphous boron carbide[12] and multiply twinned SiC[13] are due to defects rather than electrostatic interaction. In-plane spiraling can also reduce the electrostatic energy [Fig. 4(d)], resulting in the formation of nanospirals as presented in Figs. 2(a) and 2(b).

The (0001)-Zn surface has been found to be chemically active possibly due to self-catalyzed process in growth of ZnO ''comb''-like nanostructure, while the $(000\bar{1})$-O terminated surface is chemically inert.[14,15] The piezoelectric nanobelt structures may open up many possible research and applications at nanoscale, such as nanoinductors, nanospring based transducers and actuators, and tunable functional components for micro- and nano-electromechanical systems and biomedical sensing.

[1] *Nanowires and Nanobelts, Vol I: Metals and Semiconductor Nanowires; Vol. II: Nanowires and Nanobelts of Functional Materials*, edited by Z. L. Wang (Kluwer Academic, New York, 2003).

[2] Y. Cui and C. M. Lieber, Science **291**, 851 (2001).

[3] X. F. Duan, Y. Huang, R. Agarwal, and C. M. Lieber, Nature (London) **421**, 241 (2003).

[4] E. Comini, G. Faglia, G. Sberveglieri, Z. W. Pan, and Z. L. Wang, Appl. Phys. Lett. **81**, 1869 (2002).

[5] M. Arnold, P. Avouris, Z. W. Pan, and Z. L. Wang, J. Phys. Chem. B **107**, 659 (2002).

[6] Z. W. Pan, Z. R. Dai, and Z. L. Wang, Science **291**, 1947 (2001).

[7] S. C. Minne, S. R. Manalis, and C. F. Quate, Appl. Phys. Lett. **67**, 3918 (1995).

[8] C. R. Gorla, N. W. Emanetoglu, S. Liang, W. E. Mayo, Y. Lu, M. Wraback, and H. Shen, J. Appl. Phys. **85**, 2595 (1999).

[9] Y. Dai, Y. Zhang, and Z. L. Wang, Chem. Phys. Lett. **375**, 96 (2003).

[10] Z. R. Tian, J. A. Voigt, J. Liu, B. Mckenzie, and M. J. Mcdermott, J. Am. Chem. Soc. **124**, 12954 (2002).

[11] J. W. Cahn and R. E. Hanneman, Surf. Sci. **1**, 387 (1964).

[12] D. N. Mcllroy, D. Zhang, Y. Kranov, and M. Grant Norton, Appl. Phys. Lett. **79**, 1540 (2001).

[13] H.-F. Zhang, C.-M. Wang, and L.-S. Wang, Nano Lett. **2**, 941 (2002).

[14] V. Staemmler, K. Fink, B. Meyer, D. Marx, M. Kunat, S. Gil Girol, U. Burghaus, and Ch. Woll, Phys. Rev. Lett. **90**, 106102 (2003).

[15] Z. L. Wang, X. Y. Kong, and J. M. Zuo, Phys. Rev. Lett. **91**, 185502 (2003).